EFFECT ON 7 TEV PROTON BEAMS FROM THE RESIDUAL MULTIPOLAR FIELDS IN THE HL-LHC HOLLOW ELECTRON LENS*

D. Veres†, P. Geissler, P. Hermes, C. Maccani, S. Redaelli, A. Rossi, CERN, Geneva, Switzerland
G. Stancari, Fermi National Accelerator Laboratory, Batavia, Illinois, USA

Abstract

Hollow electron lenses are a promising tool for controlling beam halo at high-intensity colliders like the HL-LHC. A perfect lens can efficiently deplete particles above the inner radius of the electron beam while leaving the core – which travels through a nominally zero-field region – unaffected. However, residual multipolar fields in the electron beam and non-ideal compensations of entry and exit regions of the electron beam can lead to emittance growth and other undesired effects on the circulating-beam core. This is a particular concern for the operation with pulsed electron beam currents that ensures the fasted depletion rates. In this study, updated two-dimensional field maps from recent studies at CERN's hollow electron beam test stand are used to quantify these effects under HL-LHC conditions. Beam-dynamics simulations are performed to evaluate the emittance evolution and identify the dominant field components contributing to core degradation. The analysis also considers compensation of the dipolar component using nearby electric kicker magnets.

INTRODUCTION

The High-Luminosity LHC (HL-LHC) [1], currently planned to start operation in 2030, will run with an unprecedent stored beam energy of up to 680 MJ. LHC measurements have shown that the beam halo is generally overpopulated [2, 3]. Most recent conservative estimates based on scaling from these measurements show that up to 24 MJ could be stored in the halo above 3σ amplitude in the HL-LHC [3]. Combined with fast failure scenarios [4], such as spurious firing of beam-loss protection systems or crab cavity phase slips, that can cause sudden orbit shifts of up to 2σ, this can result in damage to the collimation system that could be mitigated by active beam halo depletion. The Hollow Electron Lens (HEL) [5, 6] was added to the original HL-LHC baseline [7] for this purpose. While removed from the latest baseline, HEL studies continued at CERN's hollow Electron Beam Test Stand (EBTS). This contribution presents beam dynamics simulations using updated two-dimensional field maps from recent EBTS measurements and simulations.

HOLLOW ELECTRON LENSES FOR BEAM HALO CLEANING IN THE HL-LHC

The HEL produces a low-energy, hollow electron beam using an annular thermionic cathode that runs coaxially to the circulating proton beam over a few meters. The electron beam is characterized by an inner and outer radius r_1 and r_2, respectively. If the electron beam is perfectly cylindrically symmetric, protons below the inner radius experience no net effect from the electrons, as the electric and magnetic fields generated by the electron current are zero. Protons at an amplitude exceeding the inner radius are subject to the electromagnetic field of the electron beam and receive a transverse kick $\theta(r)$ that depends on the protons' amplitude $r = \sqrt{x^2 + y^2}$ in the transverse plane and can be calculated for an electron beam moving in the opposite direction to the proton beam as:

$$\theta(r) = -\frac{1}{2\pi\epsilon_0}\frac{I_t L(1+\beta_e\beta_p)}{\beta_e\beta_p c^2 (B\rho)_p} f(r). \tag{1}$$

Here L is the active length of the HEL, I_t is the total electron-beam current, β_e and β_p are relativistic β-factors of the electrons and protons, respectively, $(B\rho)_p$ is the magnetic rigidity of the proton beam, and $f(r)$ is an amplitude-dependent function given by

$$f(r) = \begin{cases} 0, & \text{for } r < r_1 \\ \frac{1}{r}\frac{r^2 - r_1^2}{r_2^2 - r_1^2}, & \text{for } r_1 \le r < r_2 \\ \frac{1}{r}, & \text{for } r_2 \le r \end{cases} \tag{2}$$

The relevant parameters of the HEL are listed in Table 1.

Table 1: HL-LHC HEL Parameters.

Parameter	Value
Min. inner radius (r_1)	1.1 mm or 3.6σ
Min. outer radius (r_2)	2.2 mm or 7.2σ
Effective length (L)	3 m
Total electron current (I_t)	5 A
Relativistic β_e	0.24

The above description holds for a perfectly cylindrically symmetric, hard-edged electron beam. In practice, non-ideal compensations of the entry and exit bends of the electron beam trajectory, as well as axial asymmetries, lead to residual fields in the $r < r_1$ region. The resulting non-zero transverse kicks on the proton beam core that together with a random pulsing can cause emittance growth and core losses. The HEL can be operated in continuous, deterministic, or random pulsing modes [7]. In the random mode, the HEL is switched on and off each turn with probability p and $1 - p$, respectively. This mode offers the best halo depletion efficiency [7, 8], but has also been identified as the most critical for core emittance growth in the presence of residual fields [9] and is therefore the focus of this paper.

* Research supported by the HL-LHC project.
† dora.erzsebet.veres@cern.ch

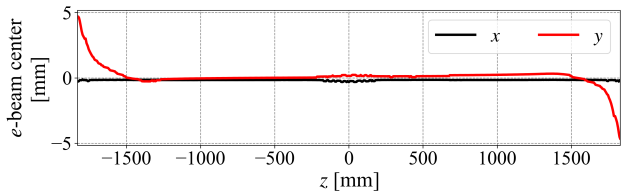

Figure 1: Electron-beam center along the HEL.

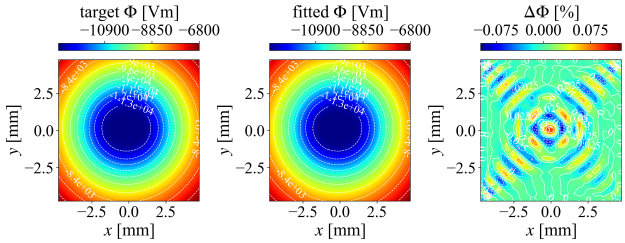

Figure 2: Comparison of the integrated electric potential of the HEL with the same reconstructed from an order 25 Chebyshev polynomial fit.

SIMULATIONS OF THE HEL EFFECT ON THE BEAM CORE

To assess the effect of residual fields inside the HEL on the beam core, a three-dimensional map of the HEL electric potential was obtained from HEL simulations done at the EBTS. While the simulated electron beam was axially symmetric, an approximately 22% imbalance was introduced between the the entry and exit corrector coil currents, as well as a longitudinal variation of the electron beam center as shown in Fig. 1.

Fast, accurate and symplectic modeling is required for long-term tracking, precluding direct numerical integration of the 3D field map. Following the approach of Ref. [10], the 3D electric potential was integrated along the longitudinal direction and the integrated potential $\Phi(x,y)$ was fitted in terms of Chebyshev polynomials $T_n(u) = \cos(n \arccos u)$ as:

$$\Phi(x,y) = \sum_{n=0}^{N} \sum_{m=0}^{n} C_{m,n-m} T_m\left(\frac{x}{a}\right) T_{n-m}\left(\frac{y}{a}\right), \quad (3)$$

where a =5 mm is a reference radius ensuring $x/a, y/a \in [-1,1]$ in the region of interest.

Figure 2 shows excellent agreement between the original and reconstructed potentials. The transverse kicks on protons below the inner radius were calculated as:

$$\theta_x(x,y) = \frac{1+\beta_e\beta_p}{\beta_p c (B\rho)_p} \frac{\partial \Phi(x,y)}{\partial x}, \qquad \theta_y(x,y) = \frac{1+\beta_e\beta_p}{\beta_p c (B\rho)_p} \frac{\partial \Phi(x,y)}{\partial y}, \quad (4)$$

while for protons above the inner radius Eqs. 1-2 were used. The resulting kick map is shown in Fig. 3, with the electron-beam center at x =−0.32 mm and y =0.15 mm taken at the middle of the HEL.

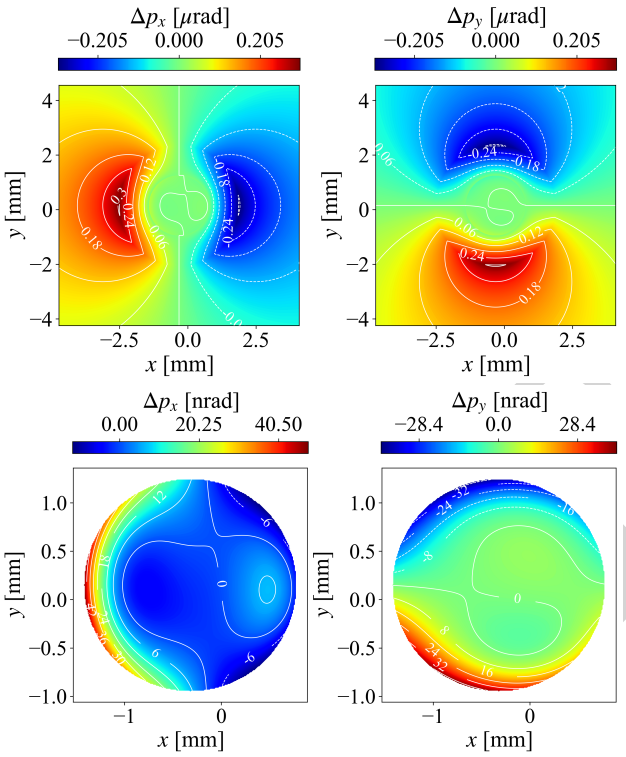

Figure 3: Transverse kicks experienced by protons passing through the HEL in the horizontal (left) and vertical (right) planes. The top panels show the kicks in the $x, y \in [-2r_2, 2r_2]$ range, while the bottom panels show the kicks for $r < r_1$.

Simulations were carried out using the `Xsuite` simulation framework [11, 12] and the latest HL-LHC optics (v1.9), at flat-top (7 TeV), with primary collimators at 6.7σ. The HEL was positioned in Insertion Region 4 with $\beta_x = \beta_y \approx$280 m, close to the transverse damper (ADT). Use of the ADT for compensation of the HEL residual kick has been proposed and studied previously assuming a purely dipolar residual kick [8, 9, 13]. Here, the ADT compensation was applied as:

$$\theta_{u,\mathrm{ADT}} = -\theta^0_{u,\mathrm{HEL}} \sqrt{\frac{\beta_{u,\mathrm{HEL}}}{\beta_{u,\mathrm{ADT}}}} \cos \Delta\mu_u, \quad \text{for } u = x, y \quad (5)$$

where $\Delta\mu_u$ is the phase advance between the ADT and the HEL in one of the transverse planes, and $\theta^0_{u,\mathrm{HEL}}$ is the HEL residual kick in the same transverse plane experienced by a proton moving on the closed orbit. The proton beam core was simulated as a 2D Gaussian distribution in both transverse planes, cut at 3σ. Single-particle tracking without machine errors of 10^5 particles was performed for 674700 turns (≈60 s) in random pulsing mode with 50% on-probability each turn. The particle distribution was monitored every 1125 turns. The simulated configurations are listed in Table 2. Figure 4 shows the survival time in initial action space and the evolution of the transverse coordinate distributions for case 5. The residual kicks induce diffusion to large amplitudes in both planes, reducing the dynamic aperture and the survival time of particles below 3σ that would otherwise

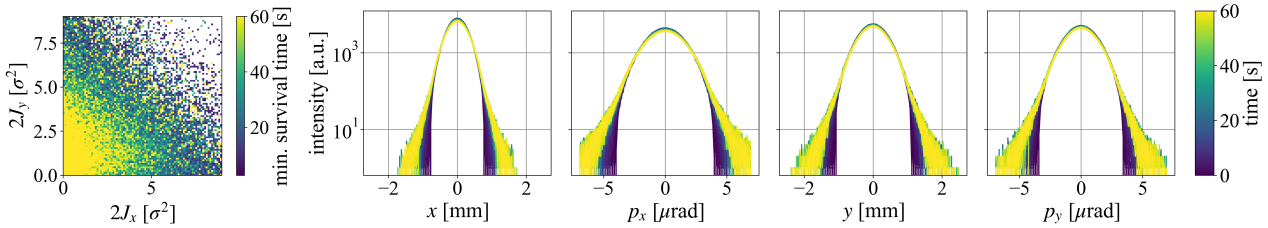

Figure 4: Particle survival time in initial action space (left) and distribution of transverse coordinates over time (right) for case 5.

Table 2: Simulated Configurations.

	HEL pulsing	**HEL residual kick**	**ADT compensation**	***p*-beam closed orbit (x[mm],y[mm])**
case 1	off	–	–	(-0.32,0.15)
case 2	random	zero	–	(-0.32,0.15)
case 3	random	constant at $(\theta_x, \theta_y) = (-2.05, 0.88)$ [nrad]	off	(-0.32,0.15)
case 4	random	constant at $(\theta_x, \theta_y) = (-2.05, 0.88)$ [nrad]	on	(-0.32,0.15)
case 5	random	from field map	off	(-0.32,0.15)
case 6	random	from field map	on	(-0.32,0.15)
case 7	random	from field map	off	(0,0)
case 8	random	from field map	on	(0,0)

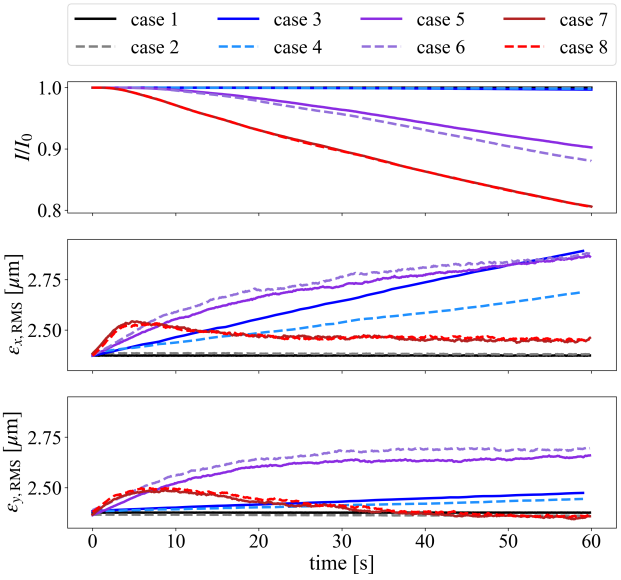

Figure 5: Simulated evolution of the beam intensity (top) and transverse normalized RMS emittances in the horizontal (middle) and vertical (bottom) planes as a function of time for different HEL residual kick and ADT compensation scenarios.

remain stable. Figure 5 shows the intensity and emittance evolution for all the different cases. The reference cases (1 and 2) show no intensity loss or emittance blow-up, as expected, and the constant-kick cases (3, 4) exhibit virtually no losses as well. However, all cases with non-constant residual kicks suffer significant beam losses – up to 20% in 60 s in the worst case – accompanied by emittance blow-up in both planes. The emittance growth is initially linear, with rates of up to 31 nm s^{-1} in the horizontal and 20 nm s^{-1} in the vertical plane for the worst cases with a misaligned proton beam (7 and 8), but slows or reverses once significant losses set in. While ADT compensation reduces these rates by 33–43% for constant kicks, it provides no benefit – and can even exacerbate losses – with the full field-map kicks, indicating that higher-order multipolar components rather than the dipolar terms are the dominant drivers.

CONCLUSIONS

The effect of residual multipolar fields in the HL-LHC hollow electron lens on the 7 TeV proton beam core was studied through long-term tracking simulations with updated 2D field maps from CERN's EBTS. In random pulsing mode, the non-uniform residual kicks inside the nominally field-free region cause significant emittance growth and beam losses over 60 s. ADT-based dipolar compensation reduces emittance growth efficiently for constant residual kicks, but is ineffective when the full amplitude-dependent kick map is applied. This demonstrates that higher-order multipolar components, rather than the dipolar field, are the primary drivers of core degradation, and highlights the necessity of good alignment of the electron beam and compensation of entry and exit effects to reduce these components. Further studies are already in progress to assess the effect of the residual kicks on the beam core in the most efficient deterministic pulsing scenarios.

REFERENCES

[1] G. Apollinari *et al.*, *High-Luminosity Large Hadron Collider (HL-LHC): Technical Design Report V.0.1*, L. Tavian, Ed. Geneva, Switzerland: CERN, 2017. doi:10.23731/CYRM-2017-004

[2] S. Papadopoulou, F. Antoniou, T. Argyropoulos, M. Fitterer, M. Hostettler, and Y. Papaphilippou, "Modelling and measurements of bunch profiles at the LHC", *J. Phys. Conf. Ser.*, vol. 874, no. 1, p. 012008, 2017. doi:10.1088/1742-6596/874/1/012008

[3] M. Rakic, "Limitations from the transverse beam halo at the high luminosity LHC and its mitigation", Ph.D. thesis, EPFL, Lausanne, Switzerland, 2026. doi:10.5075/epfl-thesis-12223

[4] B. Lindstrom *et al.*, "Fast failures in the LHC and the future high-luminosity LHC", *Phys. Rev. Accel. Beams*, vol. 23, no. 8, p. 081001, 2020. doi:10.1103/PhysRevAccelBeams.23.081001

[5] G. Stancari *et al.*, "Conceptual design of hollow electron lenses for beam halo control in the large hadron collider", CERN, Geneva, Switzerland, Rep. CERN-ACC-2014-0248, 2014. https://cds.cern.ch/record/1700455

[6] G. Stancari *et al.*, "Collimation with hollow electron beams", *Phys. Rev. Lett.*, vol. 107, no. 8, p. 084802, 2011. doi:10.1103/PhysRevLett.107.084802

[7] S. Redaelli *et al.*, "Hollow electron lenses for beam collimation at the high-luminosity large hadron collider (HL-LHC)", *J. Instrum.*, vol. 16, no. 03, P03042, 2021. doi:10.1088/1748-0221/16/03/P03042

[8] D. Mirarchi *et al.*, "Nonlinear dynamics of proton beams with hollow electron lens in the cern high-luminosity LHC", *Eur. Phys. J. Plus*, vol. 137, p. 7, 2022. doi:10.1140/epjp/s13360-021-02201-5

[9] P. Hermes *et al.*, "HL-LHC beam dynamics with hollow electron lenses", in *Proc. HB'21*, pp. 56–60, 2022. doi:10.18429/JACoW-HB2021-MOP09

[10] G. Stancari, "Calculation of the transverse kicks generated by the bends of a hollow electron lens", Fermilab, Batavia, IL, USA, Rep. FERMILAB-FN-0972-APC, 2014.

[11] G. Iadarola *et al.*, "Xsuite: an integrated beam physics simulation framework", in *Proc. HB'23*, 2024. doi:10.18429/JACoW-HB2023-TUA2I1

[12] G. Iadarola *et al.*, "Xsuite", https://xsuite.readthedocs.io/en/latest/,

[13] M. Rakic, "Compensation of residual field from hollow electron lens asymmetries in the large hadron collider", MA thesis, EPFL, Lausanne, Switzerland, 2024.